SUPERSTRUCTURE TO SUBSTRUCTURE MOMENT TRANSFER IN BEARING SUPPORTED BRIDGES

Aidcer L. Vidot –Vega, PE, Dept of Civil, Construction and Environmental Engineering, North Carolina State University, Raleigh, NC
Ben Possiel, Dept of Civil, Construction and Environmental Engineering, North Carolina State University, Raleigh, NC
Brent Robinson, **PE,** Dept of Civil, Construction and Environmental Engineering, North Carolina State University, Raleigh, NC
Mervyn Kowalsky, PhD, PE, Dept of Civil, Construction and Environmental Engineering, North Carolina State University, Raleigh, NC
Mohammed Gabr, **PhD, PE**, Dept of Civil, Construction and Environmental Engineering, North Carolina State University, Raleigh, NC

ABSTRACT

When designing bearing supported bridges with diaphragms connecting adjacent girders, it is crucial to identify the stiffness of the connection as well as its moment transfer capacity. The rotational stiffness of the connection directly impacts the assumptions of the boundary conditions and the effective length or buckling factor used in the pile or substructure design. An experimental program was performed on a typical bearing pad/diaphragm connection to study the moment transfer capabilities of bearing supported bridges. The connection was tested simulating real field conditions of NCDOT bridges. Two AASHTO Type II girders made continuous with a slab and diaphragm were utilized in the testing program. Two different sets of bearing pads were used with three different pile configurations. The axial load was varied in the bearing pads and piles while cyclic lateral load was applied to the pile in one cycle displacement increments. Test results quantify the potential of this type of connection to sustain lateral loads and flexural moments, and to develop the full strength of the pile. Test observations also show that the weakest link of this connection was the steel sole plates located at the top of the bearing pads. Rotational stiffness values for the connection were determined as a function of varying axial loads.

Keywords: Rotational stiffness, Bearing pads, Diaphragms, Moment capacity, sole plates, Bearing-supported bridges

INTRODUCTION

Bearing supported bridges with diaphragms connecting adjacent girders are widely constructed in many states, including North Carolina. There are a great variety of bearing pads, which are mechanical devices that are used to transmit the forces from the superstructure to the substructure (piles or drilled shafts). The North Carolina Department of Transportation (NCDOT) uses as a common practice elastomeric steel-laminated bearing pads in their bridges. Elastomeric bearing pads are designed to support compressive loads from the bridge superstructure and to allow horizontal movements of the beams due to thermal expansion and contraction, beam end rotations, and traffic loads. The elastomeric bearing pads are commonly specified by the degree of hardness, which is expressed in durometer points or/and by the shear modulus of the material. In this study, experimental tests were performed using two different bearing pads which differ in the durometer hardness value. The properties of the pads used in the testing program are shown in Table 1. These pads were provided by the NCDOT following their classification.

Table 1. Properties of the Bearing Pads

Type	**Durometer**	**Thickness** mm (in)	**Area** m^2 (in^2)
VI	60	63.5 (2.5)	0.1632 (253)
V	50	90.5 (3.6)	0.2097 (325)

In addition to the bearing pads, a bearing–supported connection has other important elements such as: sole plates, anchor bolts and a diaphragm connecting adjacent girders in the majority of the cases. The NCDOT bearing–supported bridge connection has the following characteristics which are similar to other states. First, the sole plates and anchor bolts connect the prestressed AASHTO girders and cap beam. Second, the bearing pads are located at the top of the cap beam, and then the sole plates are placed at the top of the bearing pad. Anchor bolts of 50.8 mm (2") diameter, which are commonly embedded 457 mm (18") into the cap beam, are bolted to the sole plates. Next, the sole plates are welded to a plate embedded in the bottom of each girder. All these elements were carefully placed during the test set up process to mimic as close as possible a real NCDOT bearing-supported bridge connection. Figures 1 show the connection details for a bearing-supported bridge, while Figure 2 schematically shows all the elements of a bearing-supported bridge connection. Figure 2 shows a side view of all the elements.

In some cases, a diaphragm is used to connect two girders together and to form a system that behaves like one unit. Figure 3 shows the reinforcing details of the concrete diaphragm used to provide continuity for two girders. These details are part of the NCDOT's common design and construction practice. The diaphragm was constructed in this way for these tests. Note that in this case, the diaphragm not only serves the usual purpose of distributing loads to

adjacent girders, but also serves to provide continuity (in conjunction with the slab) to girders along the same girder line.

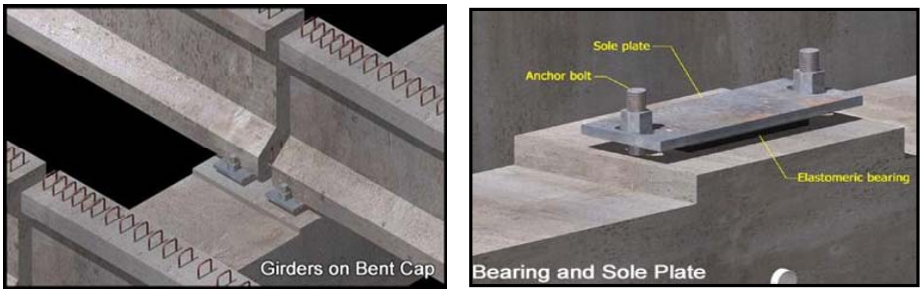

Fig. 1 Bearing- supported bridge connection details (from www.ncdot.org)

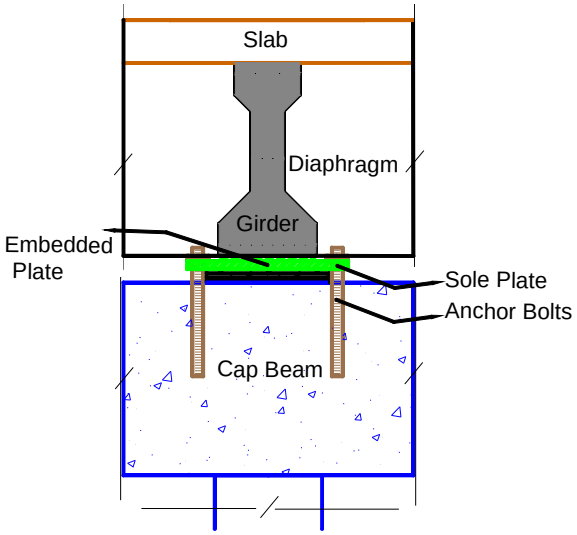

Fig. 2 Connection elements in a bearing-supported bridge (half –cut side view),

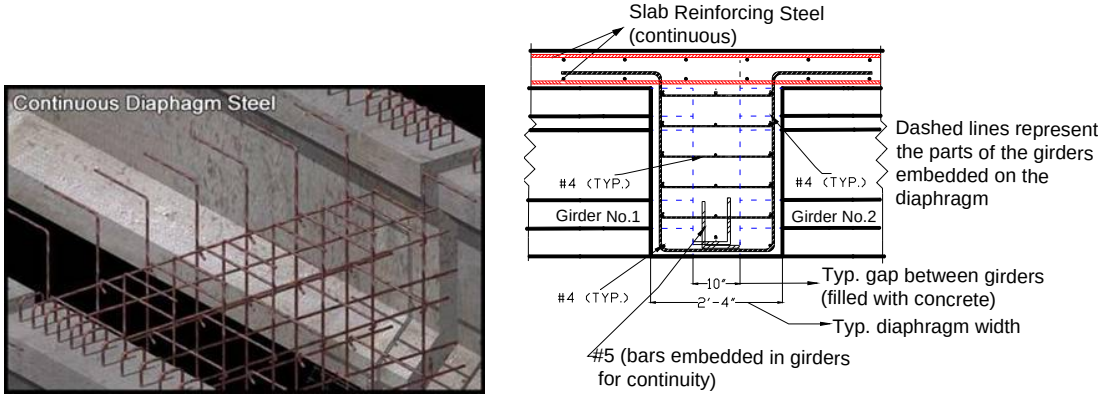

Fig. 3 (a) Girder continuity diaphragm details (from www.ncdot.org), (b) half-section through bent diaphragm

The objective of this study is to investigate the behavior of the connections in bearing–supported bridges with diaphragms connecting adjacent girders and providing continuity in conjunction with the slab to girders along the same girder line. A series of full scale tests were performed on a typical bearing pad/diaphragm connection to study the moment transfer to the piles. When a diaphragm is used to connect girders and elastomeric bearings are utilized, the potential exists for a reduced K factor, depending on the relative superstructure, connection, and substructure stiffness. This has an impact on the various design assumptions used on sizing components of bridge bents, which are very conservative in the majority of cases. These tests are part of a NCDOT project that aims to improve their current state of practice on the design of piles and drilled shaft bents.

PREVIOUS RESEARCH

Abendroth et al (1995) studied the diaphragm effectiveness in prestressed-concrete girder bridges. They tested a full scale model bridge with different intermediate diaphragm types and locations subjected to vertical and horizontal loads. The girders were supported on elastomeric bearing pads. The results from the tests were then compared with finite element models of the bridge. They determined that the vertical load distribution is independent of the type and location of the diaphragms. However, they concluded that the horizontal load distribution is dependent on the type and location of the diaphragms.

Yazdani et al (2000) studied the effects of bearing pads on the response of precast prestressed concrete bridges. They concluded that performance characteristics of AASHTO precast bridge I beams are slightly enhanced by the effects of restraints from laminated neoprene bearing pads. These performance characteristics include: mid-span deflection, tensile and compressive stresses, horizontal restraint forces, and end moments. These effects increase at cold temperatures due to stiffening of the pads, but such increases are minimal. Also, they found out that the horizontal restraint forces transmitted by the bearing pads to the substructure are small, generally within AASHTO limits for the bridge under this study.

Eamon and Nowak (2001) conducted research on the effects of secondary elements such as barriers, sidewalks and diaphragms on bridge structural system reliability considering moment capacity. They determined that these elements can affect the live load distribution and increase the bridge load carrying capacity. The use of typical combinations of secondary systems has varying effects on girder reliability. In addition, the use of diaphragms was shown to be more effective for increasing the load distribution for bridges with wider girder spacing. The effects of secondary elements are more pronounced on live load distribution, when the span length increases.

Green et al (2004) modeled a Florida Bulb Tee 78 precast concrete bridge girder, which is widely used in the state of Florida to determine the effects of intermediate diaphragms and bearing stiffness on the performance of prestressed AASHTO type bridge girders. This study indicated that the presence of intermediate diaphragms stiffens the precast prestressed girders

and reduces the maximum girder deflection. Also, increasing bearing pad stiffness leads to stiffening of the girders, but this is generally small in magnitude.

Yoon et al (2004) studied the behavior of sole plates in elastomeric bearing systems supporting steel box and/or plates girders. In these types of girders, the bottom flange and the sole plate may act together in dispersing concentrated stresses. The sole plates are important to resist compression and flexural stresses due to bending of the girder and local stress concentration in the diaphragm area. The authors developed several finite element models of the elastomeric bearing system (bearing pads, sole plates, diaphragm and girders) for this study. It was found that the sole plate thickness affects the stresses in both the bottom flange immediately under the diaphragm and elastomeric bearing pads. Therefore, the sole plate needs to have an appropriate thickness to control the stress concentration in the bottom flange of the girder and to limit stresses in the elastomeric bearing pads.

In general, previous studies have focused on a particular component of the bearing-supported connection systems. Nearly, all of the researchers have studied the diaphragm and bearing pad behavior related to load distributions and girder deflection. No one, to the authors' knowledge have studied the moment capabilities of bearing-supported connection systems and tested all the elements of the connection together including the pile or substructure elements.

OVERVIEW OF EXPERIMENTAL PROGRAM

The experimental program consisted of a total of 42 tests on a bearing-supported bridge connection. The connection was tested upside down as shown in Fig. 4 to simplify the set- up and testing process in the laboratory environment. The setup consisted of a steel frame in which a 979 kN (220 kip) actuator was connected (Nos. 1 and 2 on Fig. 4). The actuator was used to apply the lateral load during the tests. The steel frame was rigidly attached to the laboratory strong floor using four 35 mm (1-3/8") dywidag bars. An additional bracing system was provided for lateral stability. Five (5) 534 kN (60 ton) jacks were used to apply axial loads to the column (No. 3) and bearing pads (No. 4) to simulate gravity effects. The axial load at the bearing pads was distributed by the use of two HSS beams at each bearing pad location (No. 5 on Fig. 4). This can be observed in detail on Figure 6b. The control of the axial load on the bearing pads and column was made by the use of two separate hydraulic pumps, each one having a pressure valve. The axial load was applied to the bearing pads separately from the column load because usually one set of bearings sheds load to several piles, and this can be accounted for by applying the load directly to the cap beam.

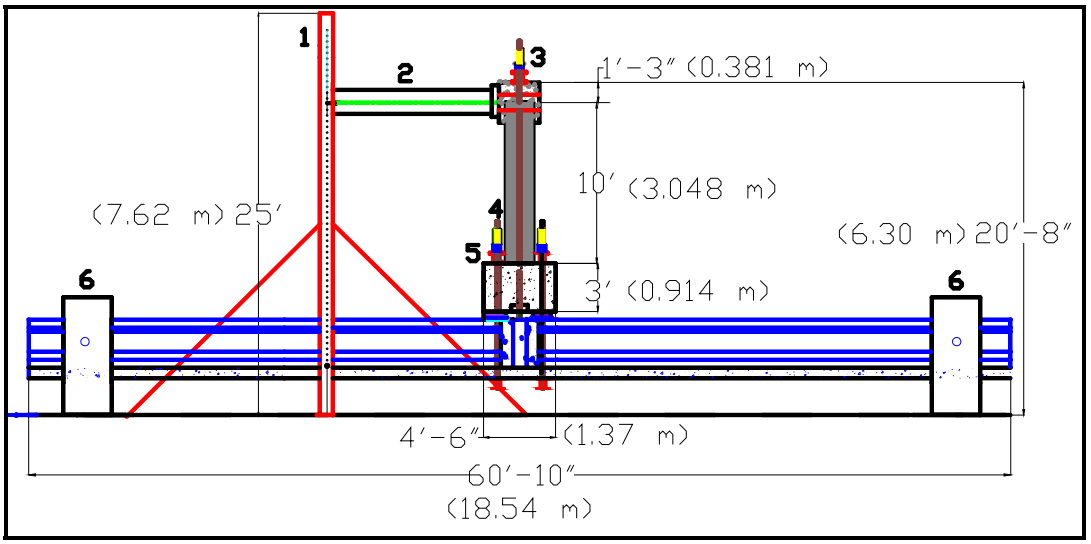

Fig. 4 Experimental test set-up (lateral view)

The girder ends were connected by means of a pinned connection. This pinned connection at girder ends consisted of two L-shape concrete blocks at each end and a steel rod of 127 mm (5 in) diameter (No. 6 on Fig. 3). Two AASHTO Type II girders 9.14 m (30 ft) long were used during the tests. The girders were made continuous with a diaphragm and slab, following the NCDOT specifications. The girder ends have two L-shape bars that extend around 254 mm (10 in) horizontally and 177.8 (7 in) vertically (see Figure 3). The reinforcing steel around the diaphragm consisted of several longitudinal bars running all the way through it and some stirrups that are extended into the deck slab. Three different pile configurations of 3.048 m (10 ft) length were tested to simulate a range of substructure stiffnesses and shapes commonly used in practice. The piles included a circular and square reinforced concrete, and a steel HP-pile section. The circular pile had a diameter of 457 mm (18 in) and the square pile dimensions were 508 x 508 mm (20 x 20 in). Fig. 5 shows the three pile sections used during the experimental program. Figure 6 (a,b) shows a photograph of the overall testing set up including the system used to apply axial loads to the pile and bearing pad independently.

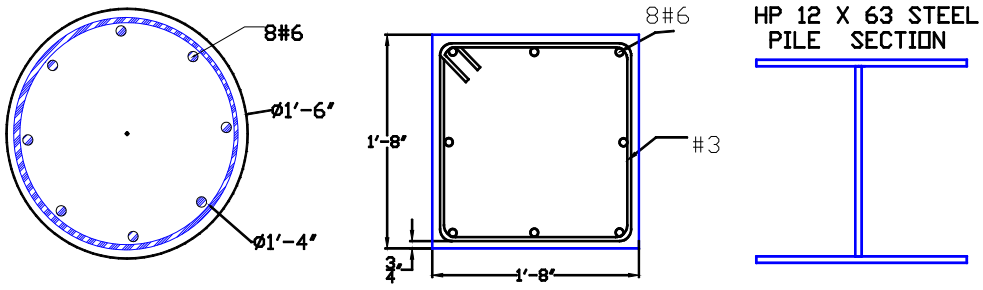

Fig. 5 Pile Sections

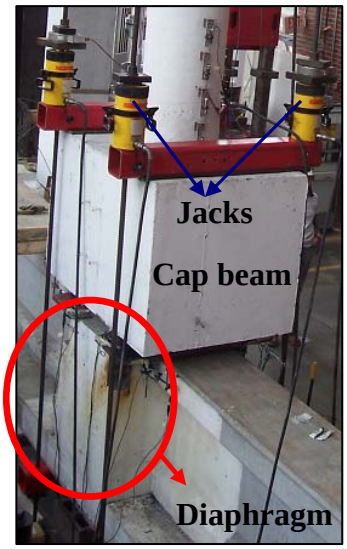

Fig. 6 a –b Test set-up view (a) and jacks used to applied axial load at the bearing pads (b)

INSTRUMENTATION

The data monitoring sensors included 55 instruments. Three load cells were used to monitor the axial load in the bearing pads and pile. String pots were used to measure displacements at the bottom of the slab/girder, at the cap beam, and top of the pile. Linear potentiometers were used to measure displacements at the base of the pile, and compression and shear deformations of the bearing pads. In addition, linear potentiometers were use to measure any displacement/slippage of the bearing pads in the transverse direction to the lateral load. Twelve strain gages were use to monitor the strain in the longitudinal reinforcing bars near the pile-cap beam interface in the circular and square pile sections. Finally, three inclinometers were used to measure rotation at the diaphragm, top of the pile and cap beam.

TEST MATRIX AND LOADING PROTOCOL

A total of 42 tests were performed to different piles and bearing pad types, as shown in the test matrix in Fig. 7. Only the two concrete piles were subjected to three different levels of axial load ratio (ALR) in an attempt to model substructures of different stiffness. The axial load ratio (ALR) is defined as:

$$ALR = \frac{P}{f_c' A_{gross}} \quad (1)$$

where P is the axial load on the pile, f'_c is the compressive concrete strength and A_{gross} the gross area of the pile section. In addition, for each ALR in the pile, the axial load at the bearing pads was varied three times (P1, P2, P3). This was performed for each bearing

pad/pile combination. Axial loads were applied to the column and bearing pads to simulate gravity effects. Table 2 to 4 show the axial loads used on the piles and bearing pads.

Table 2 Loads for circular pile cases

Case	ALR (%)	Pile	Load on one Bearing Pad		
		P kips (kN)	**P1** kips (kN)	**P2** kips (kN)	**P3** kips (kN)
1	**4**	46 (205)	11 (51)	17 (76)	23 (102)
2	**6**	69 (307)	17 (76)	26 (116)	34 (151)
3	**8**	92 (409)	23 (102)	34 (151)	46 (205)

Table 3 Loads for square pile cases

Case	ALR (%)	Pile	Load on one Bearing Pad		
		P kips (kN)	**P1** kips (kN)	**P2** kips (kN)	**P3** kips (kN)
1	**3**	54 (240)	13.5 (60)	20 (89)	27 (120)
2	**4**	72 (320)	18 (80)	27 (120)	36 (160)
3	**5**	90 (400)	23 (102)	34 (151)	45 (200)

Table 4 Loads for HP pile cases

Case	Pile	Load on one Bearing Pad		
	$P_{assumed}$ kips (kN)	**P1** kips (kN)	**P2** kips (kN)	**P3** kips (kN)
1	109 (485)	27 (120)	41 (182)	55 (245)

Three different axial load ratios (ALR) were applied (0.04, 0.06 and 0.08) to the circular pile as shown in Table 2. The axial load ratios were changed to 0.03, 0.04 and 0.05 for the square pile (Table 3). This was due to limitations associated with the yield force of the bar and load cell capacity which would have been exceeded with the use of 6 or higher axial load percentage in this column. The relationship between the axial loads in the pile to the axial load in the bearing pads was done by comparing the loads applied to bearing pads to the loads transferred to the piles for four bridge case studies presented in Robinson et al. (2006). Note that the HP Pile was tested without pile axial load, as the stiffness of that section should not be dependent on axial load. The target loads were monitored during each test with load cells. A summary of the testing program is schematically illustrated in Fig 7, together with the number of specimens tested on Table 5 for each bearing pad (Type V and VI).

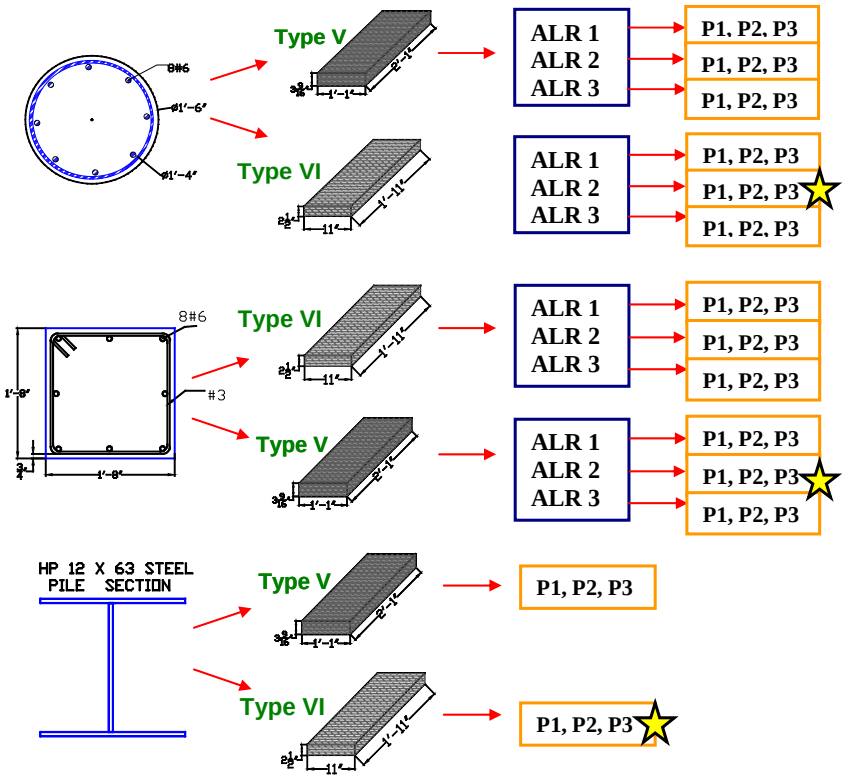

Fig. 7 Test Matrix

Table 5 Number of specimens tested under the experimental program (for each bearing pad)

Specimen Nomenclature									
Pile	**Square Pile**			**Circular Pile**			**HP Pile**		
Axial load on pad	**P1**	**P2**	**P3**	**P1**	**P2**	**P3**	**P1**	**P2**	**P3**
ALR 1 (pile)	S3-BP1	S3-BP2	S3-BP3	C4-BP1	C4-BP2	C4-BP3	HP-BP1	HP-BP2	HP-BP3
ALR 2 (pile)	S4-BP1	S4-BP2	S4-BP3	C6-BP1	C6-BP2	C6-BP3			
ALR 3 (pile)	S5-BP1	S5-BP2	S5-BP3	C8-BP1	C8-BP2	C8-BP3			

The axial loads on the bearing pads increased from the target load as the lateral load increased during the test. Figure 8 shows the variation of the axial load on one bearing pad for case S3-BP1 (square pile with P1 load on bearing pad). This situation was similar for all cases.

In addition to the axial loads, cyclic lateral loads were applied to all specimens. The lateral loading history for all the tests consisted of reversed single displacement cycles in increments of 19 mm (0.75 inches) until the yield displacement for each case. The yield displacement was defined as the top pile displacement at which the theoretical first yield force was achieved in each pile section. The square and circular pile yield displacement was 76 mm (3"). For the HP pile, the yield displacement occurred at 152 mm (6.0"). In addition, each

pile was subjected to inelastic cycles (cases with a star in Fig. 7).The loading history is shown in Fig. 9a-b.

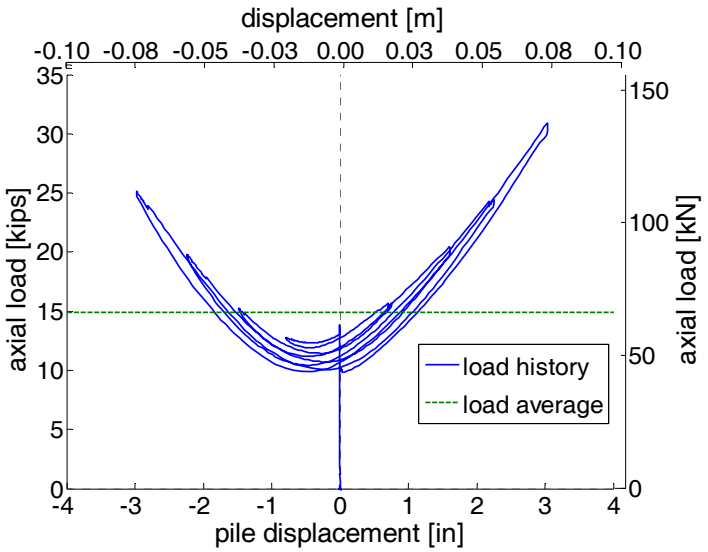

Fig. 8 Axial Load vs. pile displacement (S3-BP1 case)

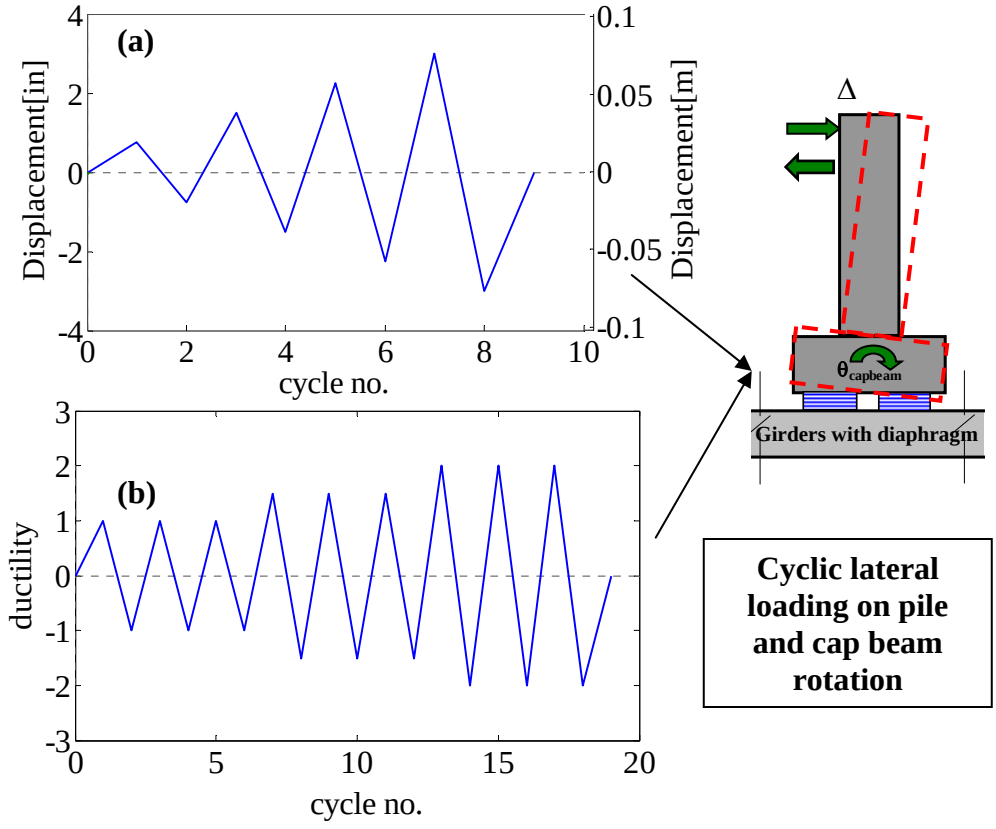

Fig. 9 Loading Protocol (a) elastic cycles (b) inelastic cycles

TESTING RESULTS

Figures10 to 12 present the hysteretic responses for the cases in which the pile was subjected to displacements that exceed the yield of the pile (ductility cases in Figure 7). These cases included: square pile with Type V bearing pad, circular pile with Type VI bearing pad and HP pile with Type VI bearing pad. These figures show the force vs. pile top displacement and moment as a function of the cap beam rotation responses. The circular pile was subjected to the first loading protocol (Figure 9a) and to three ductility cycles of 1 to 1.5 (Figure 9b). The square pile was subjected to an additional cycle in the push direction of ductility 2 (displacement of 166 mm (6.52 in)). The HP pile was displaced until 237 mm (9.34 in).

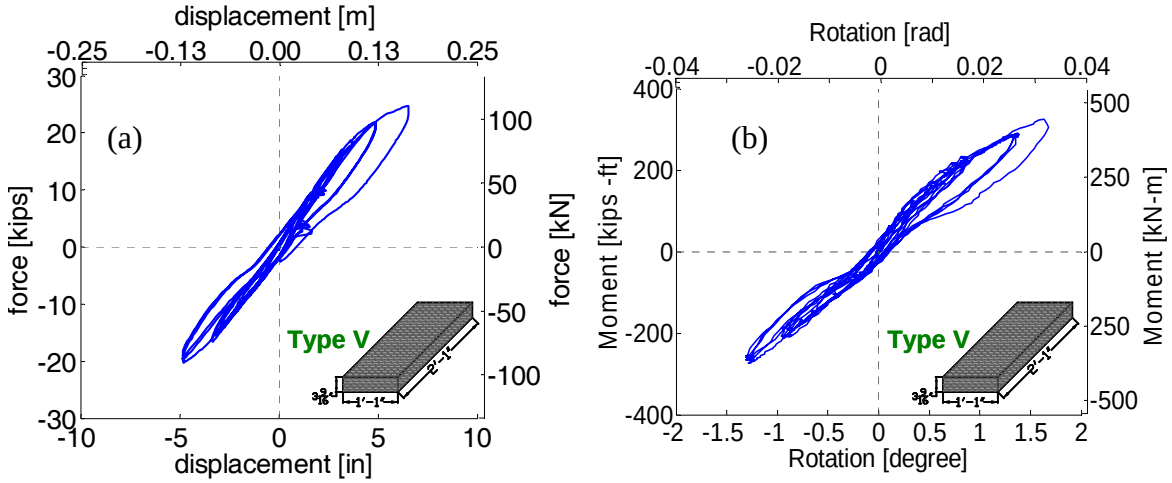

Fig. 10 (a) Force-displacement response for square pile 4% ALR/P3 (b) Moment vs. cap beam rotation

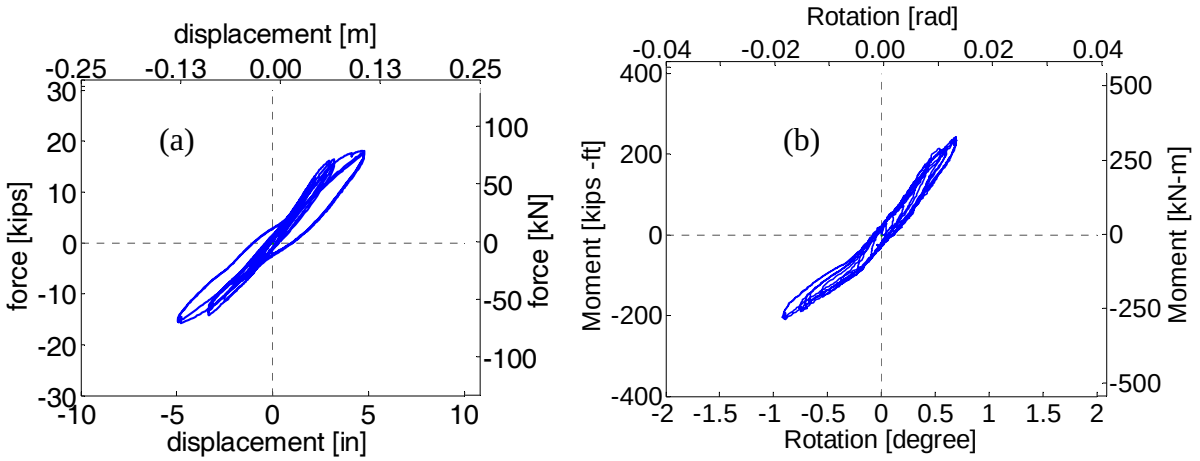

Fig. 11 (a) Force-displacement response for circular pile 6% ALR/P3 bearing pad load (b) Moment vs. cap beam rotation

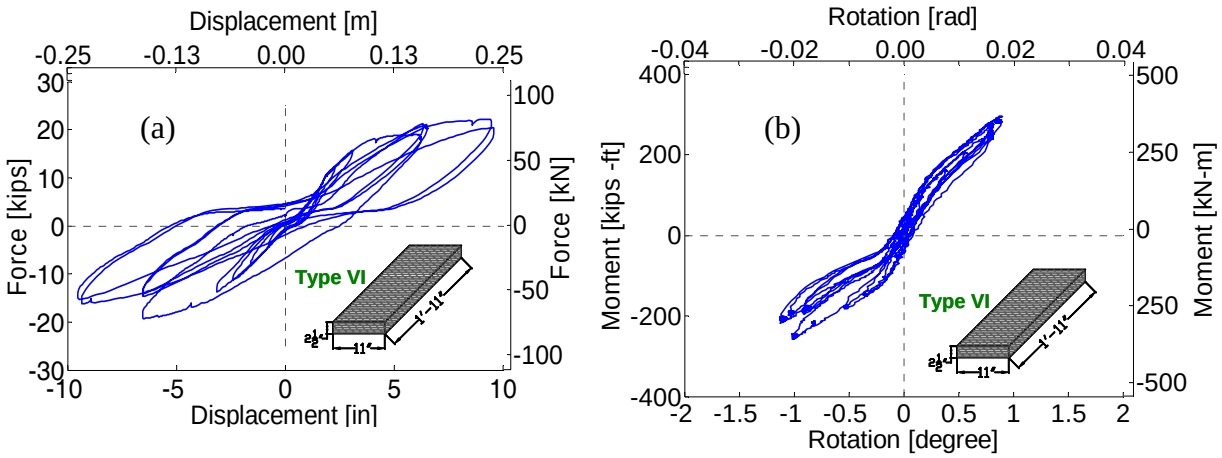

Fig. 12 Force-displacement response for HP pile/P3 (b) Moment vs. cap beam rotation

In general, similar responses were obtained in all cases. An increase in lateral applied force (albeit slight at times) was observed with the increase of the axial load at the bearing pads. This situation was expected, as well as the increase in lateral force needed to attain a certain level of displacement when the connection was tested with the Type VI bearing pad, which is the stiffer of the two. As the axial load increases, the concrete piles and bearing pads become stiffer.

Table 6 shows maximum values of pile displacement (Δ_{max}), rotation of cap beam ($\theta_{capbeam(max)}$) and applied moment ($M_{applied}$) for all the cases in the push direction only. Also shown in Table 6, is the average axial load on the pile (P_{column}) and one bearing pad (P_{bp}) for all tests. It can be noticed that the rotation at the cap beam is very similar for the cases with square and circular piles. The maximum moment applied for the inelastic cases varied between 445 kN-m (328 kips-ft) for the square pile with Type V pad, 316 kN-m (233 kips-ft) for the circular pile with Type VI pad, and 331 kN-m (244 kips-ft) for the HP pile with Type VI pad.

Accordingly, it seems that this type of connection is able to take a substantial magnitude of moment without the complete failure of all connection elements. The weakest link in the connection was found to be the steel sole plates that are located at the top of the bearing pads. The soles plates experienced bending about their weak axis around the first cycles of ductility 1.5 for the cases with circular and square piles. The plates bent approximately by ½ in (12.7 mm) at both sides during the end of the load history. The same situation occurred for the cases with the HP pile. The prying action of the embedded part of the HP pile caused large damage in the cap beam and the test was stopped at 9.34 inches (237 mm). Figures 13 (a)-(d) show several pictures depicting crushing of the concrete on the area of the embedded and sole plates (a), bending of the sole plates (b and c), and prying action at the cap beam of the HP pile (d).

(a)

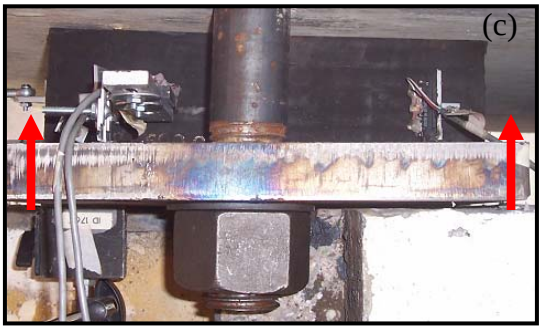

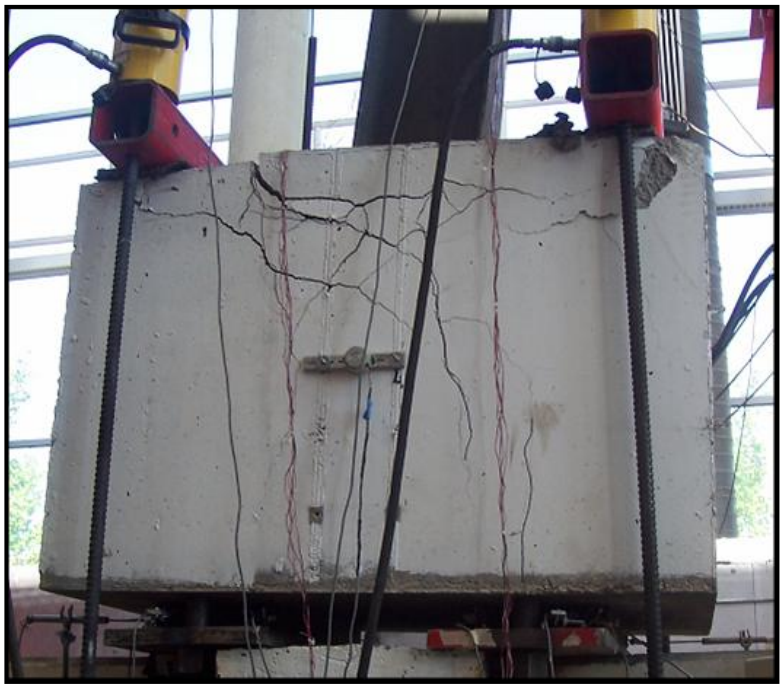

(d)

Fig. 13 (a) crushing of concrete at the plates area, (b) bending of sole plates (side view), (c) bending of the sole plates (front view),and (d) failure of the cap beam area (HP pile)

Table 6 Maximum displacement, rotation and moment for push direction and average axial load on piles and bearing pads

Bearing Pad Type	V	VI	V		VI		V		VI		V	VI	V		VI	
Case	$\Delta_{topcolumn\ (max)}$ mm (in)		$P_{column\ (average)}$ kN (kips)				$P_{bp\ (average)}$ kN (kips)				$\theta_{capbeam\ (max)}$ (degree)		$M_{applied\ (max)}$ kN-m (kips-ft)			
S3-BP1	75.67 (2.98)	80.95 (3.19)	241.30	(54.23)	241.30	(54.23)	85.8	(19.28)	85.08	(19.12)	0.69	0.78	220.06	(162.20)	247.46	(182.40)
S3-BP2	75.67 (2.98)	76.39 (3.01)	244.69	(54.99)	244.69	(54.99)	137.4	(30.87)	137.18	(30.83)	0.66	0.69	243.66	(179.60)	231.18	(170.40)
S3-BP3	75.67 (2.98)	75.67 (2.98)	247.25	(55.56)	247.31	(55.58)	167.7	(37.68)	167.04	(37.54)	0.62	0.67	259.95	(191.60)	256.42	(189.00)
S4-BP1	75.99 (2.99)	76.08 (3.00)	326.07	(73.28)	332.08	(74.63)	113.6	(25.52)	140.62	(31.60)	0.67	0.68	240.00	(176.90)	265.51	(195.70)
S4-BP2	75.99 (2.99)	76.08 (3.00)	325.85	(73.23)	332.58	(74.74)	155.9	(35.04)	168.38	(37.84)	0.64	0.64	263.61	(194.30)	288.98	(213.00)
S4-BP3	75.67 (2.98)	75.99 (2.99)	330.08	(74.18)	333.86	(75.03)	201.5	(45.29)	209.37	(47.05)	0.61	0.61	285.45	(210.40)	310.69	(229.00)
S4-BP3_inelastic	169.93 (6.69)	-	336.95	(75.72)	-		217.3	(48.83)	-		1.33	-	445.47	(328.35)	-	
S5-BP1	75.67 (2.98)	75.99 (2.99)	400.61	(90.03)	399.05	(89.68)	140.1	(31.48)	141.844	(31.88)	0.65	0.67	250.86	(184.90)	279.89	(206.30)
S5-BP2	75.99 (2.99)	69.70 (2.74)	399.50	(89.78)	393.49	(88.43)	187.5	(42.14)	194.632	(43.74)	0.63	0.58	290.88	(214.40)	301.60	(222.30)
S5-BP3	75.99 (2.99)	72.42 (2.85)	399.22	(89.71)	399.00	(89.66)	236.2	(53.09)	243.86	(54.80)	0.61	0.58	307.29	(226.50)	321.54	(237.00)
C4-BP1	65.53 (2.58)	67.82 (2.67)	209.79	(47.14)	207.04	(46.52)	65.55	(14.73)	69.33	(15.58)	0.65	0.66	153.99	(113.50)	147.34	(108.60)
C4-BP2	64.77 (2.55)	67.06 (2.64)	207.85	(46.70)	206.75	(46.46)	98.97	(22.24)	101.90	(22.89)	0.60	0.66	164.30	(121.10)	152.22	(112.20)
C4-BP3	64.52 (2.54)	65.53 (2.58)	209.09	(46.99)	207.58	(46.64)	123.12	(27.67)	124.30	(27.93)	0.56	0.58	166.74	(122.90)	168.64	(124.30)
C6-BP1	63.50 (2.50)	66.04 (2.60)	309.01	(69.44)	314.59	(70.69)	94.36	(21.21)	102.33	(22.99)	0.56	0.54	171.22	(126.20)	172.98	(127.50)
C6-BP2	62.99 (2.48)	64.52 (2.54)	311.36	(69.99)	309.70	(69.59)	136.70	(30.72)	138.41	(31.10)	0.55	0.53	178.95	(131.90)	191.43	(141.10)
C6-BP3	61.72 (2.43)	62.64 (2.47)	315.69	(70.94)	310.01	(69.67)	170.70	(38.36)	171.24	(38.48)	0.51	0.46	185.46	(136.70)	213.14	(157.10)
C6-BP3_inelastic	-	120.90 (4.76)	-		381.77	(85.79)	-		244.21	(54.88)	-	0.90	-		316.29	(233.13)
C8-BP1	62.48 (2.46)	66.29 (2.61)	397.77	(89.39)	411.62	(92.49)	135.28	(30.40)	130.57	(29.34)	0.52	0.50	183.70	(135.40)	195.09	(143.80)
C8-BP2	61.21 (2.41)	64.52 (2.54)	395.80	(88.94)	410.30	(92.20)	169.22	(38.03)	173.55	(38.99)	0.49	0.49	194.55	(143.40)	214.90	(158.40)
C8-BP3	59.69 (2.35)	63.50 (2.50)	395.91	(88.97)	407.88	(91.65)	218.27	(49.05)	221.65	(49.81)	0.44	0.41	199.98	(147.40)	236.61	(174.40)
HP-BP1	76.71 (3.02)	76.45 (3.01)	-		-		143.1	(32.17)	142.01	(31.91)	1.66	0.52	238.17	(175.55)	225.76	(166.41)
HP-BP2	76.71 (3.02)	76.45 (3.01)	-		-		204.3	(45.90)	207.29	(46.58)	1.24	0.47	265.45	(195.66)	260.08	(191.70)
HP-BP3	76.08 (3.00)	78.49 (3.09)	-		-		252.6	(56.76)	261.56	(58.78)	1.16	0.45	281.81	(207.72)	279.95	(206.34)
HP-BP3_inelastic	-	243.84 (9.59)	-		-		-		262.01	(58.88)	-	0.93	-		330.96	(243.94)

* S—Square concrete, C—Circular concrete, HP—H-Pile, BP—Bearing Pad

Figures 14 to 18 present the secant rotational stiffness ($K_\theta = M/\theta$) for the connection under study with the different pile and bearing pad combinations. Fig. 14 and Fig. 15 show the values for the connection with square pile/Type V and Type VI pad with different levels of axial load ratio on the pile (S3 to S5) and three different levels of axial load on the pads (BP1, BP2, BP3). Fig. 16 and Fig. 17 present the values for the connection with circular pile/Type V and Type VI pad with different level of axial load ratio on the pile (C4, C6 and C8) and three different levels of axial load on the pads (BP1, BP2, BP3). Later, Figure 18 shows the stiffness values for the HP pile cases.

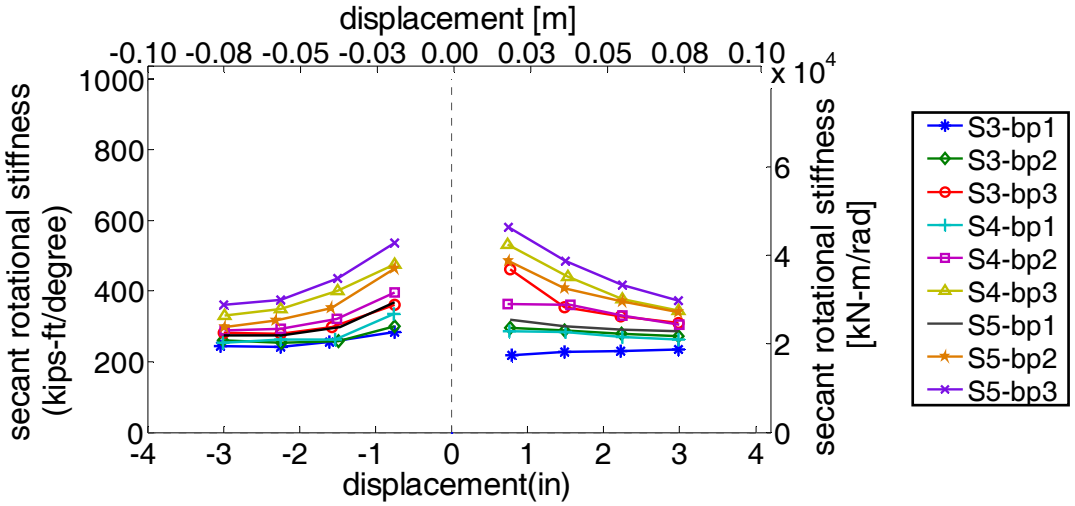

Fig. 14 Secant rotational stiffness of connection with square pile for different axial load combinations (bp1, bp2, bp3 on Type V pad)

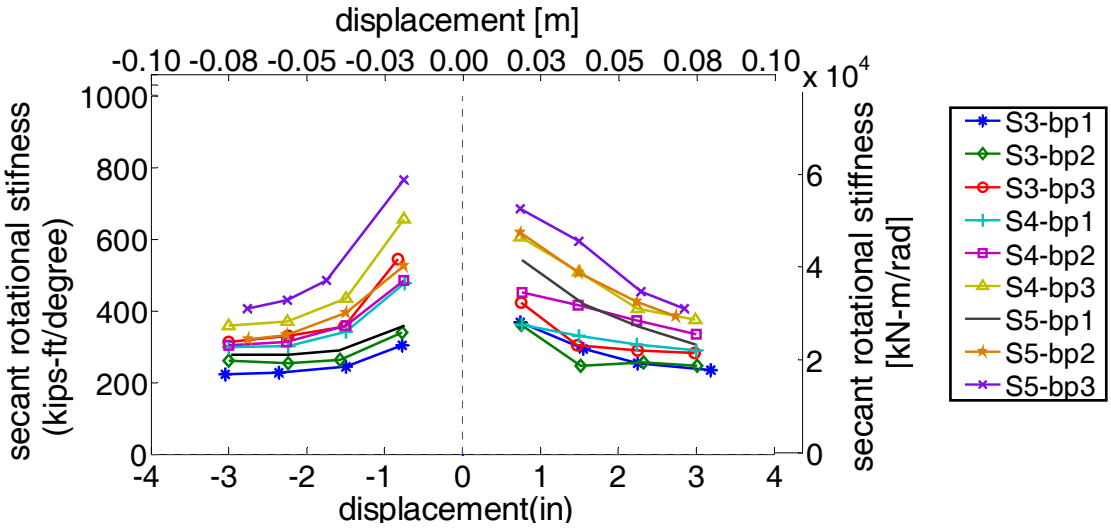

Fig. 15 Secant rotational stiffness of connection with square pile for different axial load combinations (bp1, bp2, bp3 on Type VI pad)

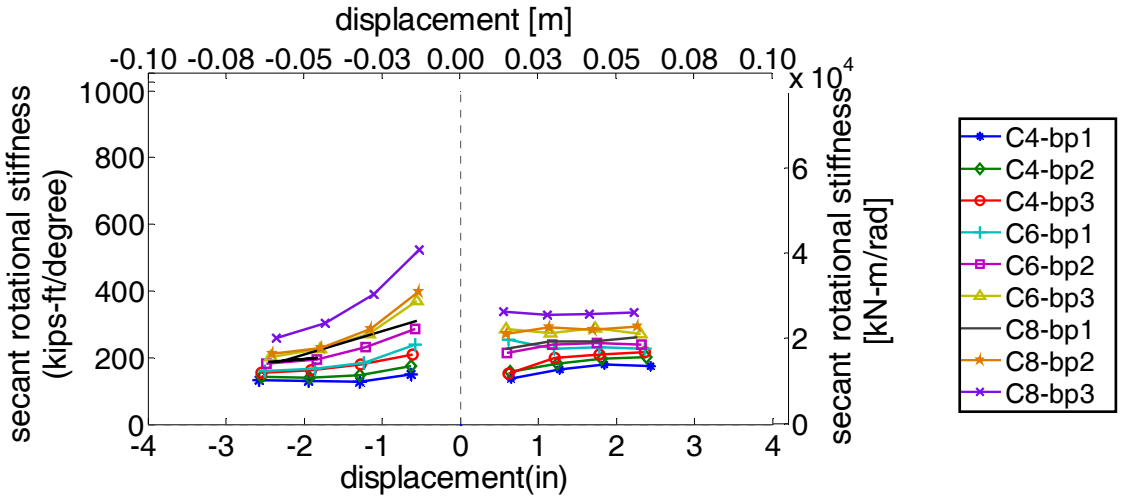

Fig. 16 Secant rotational stiffness of connection with circular pile for different axial load combinations (bp1, bp2, bp3 on Type V pad)

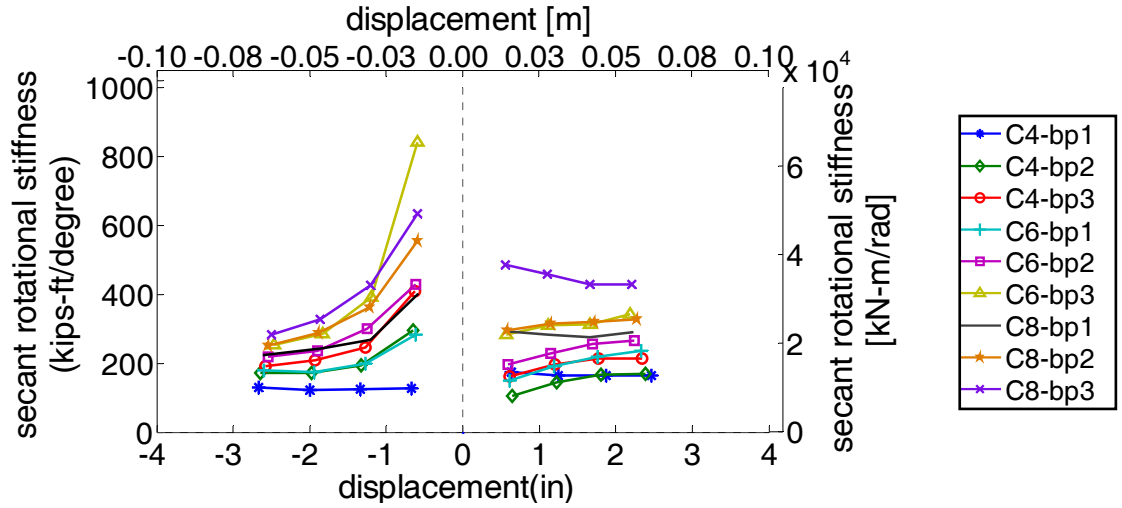

Fig. 17 Secant rotational stiffness of connection with circular pile for different axial load combinations (bp1, bp2, bp3 on Type VI pad)

It can be noticed that the secant rotational stiffness is higher for the square pile cases and for cases with Type VI pad. The square pile is stiffer than both the circular and HP piles, which is contributing more to the stiffness of the connection. Similarly, the type VI pad has a higher shear modulus which provides a higher resistance to the lateral force, increasing the stiffness of the connection. For the circular pile, the rotational stiffness is lower in the push direction as higher rotations were experienced in this direction. This could have happened due to the unleveled surface of the bottom of the cap beam acquired during the casting process. As the axial load on the bearing pad and pile increases, the stiffness also increases. Tables 7 to 11 present the values of the rotational stiffness for selected cases at different cycles in push and pull directions for the elastic cases only (4 cycles until 3 in (76 mm) of displacement). The

differences between the rotational stiffness using Type V and Type VI bearing pads are more evident on the HP pile cases. There are significant differences between the rotational stiffness for the HP specimens with the different types of bearing pads used during these tests (Table 11).

Table 7 Secant rotational stiffness for connection with square pile /Type V pad

Secant Rotational Stiffness [MN-m/rad (Kips-ft/degree)]												
Cycle No.	S3-BP1		S3-BP3		S4-BP1		S4-BP3		S5-BP1		S5-BP3	
1 (push)	16.93	(217.77)	35.80	(460.51)	22.20	(285.54)	41.30	(531.34)	24.77	(318.63)	45.17	(581.11)
1 (pull)	22.08	(284.07)	28.07	(361.13)	26.01	(334.61)	36.94	(475.21)	28.69	(369.15)	41.59	(535.05)
2 (push)	17.65	(227.09)	27.49	(353.71)	22.03	(283.43)	34.22	(440.25)	23.31	(299.82)	37.64	(484.22)
2 (pull)	19.96	(256.78)	23.07	(296.82)	20.43	(262.88)	31.18	(401.07)	23.19	(298.29)	33.87	(435.77)
3 (push)	17.83	(229.43)	25.56	(328.88)	21.07	(271.02)	29.39	(378.06)	22.66	(291.45)	32.35	(416.22)
3 (pull)	18.72	(240.88)	21.79	(280.36)	20.48	(263.47)	27.11	(348.79)	21.26	(273.54)	29.22	(375.85)
4 (push)	18.21	(234.32)	23.99	(308.59)	20.49	(263.63)	26.86	(345.48)	22.18	(285.39)	28.91	(371.88)
4 (pull)	19.04	(244.97)	21.81	(280.54)	19.72	(253.65)	25.66	(330.04)	21.35	(274.63)	27.99	(360.09)

Table 8 Secant rotational stiffness for connection with square pile /Type VI pad

Secant Rotational Stiffness [MN-m/rad (Kips-ft/degree)]												
Cycle No.	S3-BP1		S3-BP3		S4-BP1		S4-BP3		S5-BP1		S5-BP3	
1 (push)	28.62	(368.14)	32.92	(423.48)	27.98	(359.99)	47.10	(605.95)	42.18	(542.59)	53.27	(685.30)
1 (pull)	23.55	(302.99)	42.29	(544.08)	37.12	(477.51)	50.91	(654.98)	27.94	(359.44)	59.46	(764.90)
2 (push)	22.89	(294.40)	23.64	(304.09)	25.59	(329.19)	39.50	(508.15)	32.46	(417.63)	46.23	(594.69)
2 (pull)	18.88	(242.94)	27.61	(355.14)	26.52	(341.11)	33.81	(435.00)	22.44	(288.73)	37.66	(484.46)
3 (push)	19.66	(252.89)	22.55	(290.11)	23.82	(306.37)	31.47	(404.89)	27.74	(356.89)	35.35	(454.72)
3 (pull)	17.71	(227.89)	25.59	(329.20)	23.39	(300.95)	28.80	(370.43)	21.65	(278.51)	33.32	(428.66)
4 (push)	18.25	(234.72)	21.90	(281.73)	22.50	(289.49)	29.08	(374.14)	23.83	(306.60)	31.60	(406.45)
4 (pull)	17.39	(223.74)	24.25	(311.98)	23.28	(299.48)	27.85	(358.24)	21.58	(277.67)	31.64	(406.98)

Table 9 Secant rotational stiffness for connection with circular pile /Type V pad

Secant Rotational Stiffness [MN-m/rad (Kips-ft/degree)]												
Cycle No.	C4-BP1		C4-BP3		C6-BP1		C6-BP3		C8-BP1		C8-BP3	
1 (push)	10.74	(138.19)	11.78	(151.52)	19.69	(253.36)	22.23	(286.02)	17.54	(225.65)	26.17	(336.72)
1 (pull)	11.68	(150.20)	16.21	(208.55)	18.61	(239.42)	28.85	(371.11)	24.18	(311.02)	40.76	(524.32)
2 (push)	12.80	(164.72)	15.54	(199.87)	17.51	(225.27)	21.32	(274.21)	19.31	(248.38)	25.57	(328.93)
2 (pull)	9.94	(127.90)	13.94	(179.38)	14.26	(183.46)	21.12	(271.64)	14.79	(190.25)	30.27	(389.45)
3 (push)	13.87	(178.39)	16.21	(208.52)	17.96	(230.99)	22.36	(287.63)	19.32	(248.59)	25.69	(330.51)
3 (pull)	10.15	(130.56)	12.51	(160.92)	13.04	(167.70)	17.56	(225.84)	15.41	(198.24)	23.49	(302.24)
4 (push)	13.60	(174.89)	16.76	(215.59)	17.59	(226.23)	21.00	(270.14)	20.27	(260.79)	26.04	(335.03)
4 (pull)	10.24	(131.71)	12.06	(155.19)	12.44	(160.04)	15.74	(202.55)	14.55	(187.20)	20.05	(257.89)

Table 10 Secant rotational stiffness for connection with circular pile /Type VI pad

Secant Rotational Stiffness [MN-m/rad (Kips-ft/degree)]												
Cycle No.	C4-BP1		C4-BP3		C6-BP1		C6-BP3		C8-BP1		C8-BP3	
1 (push)	13.45	(172.98)	12.54	(161.32)	11.60	(149.26)	22.06	(283.77)	22.77	(292.88)	37.68	(484.68)
1 (pull)	9.83	(126.50)	31.82	(409.40)	22.05	(283.69)	65.35	(840.66)	31.13	(400.52)	49.30	(634.16)
2 (push)	12.68	(163.13)	15.27	(196.44)	14.87	(191.31)	24.08	(309.78)	21.96	(282.45)	35.60	(457.95)
2 (pull)	9.65	(124.09)	19.13	(246.16)	15.49	(199.29)	30.45	(391.71)	20.80	(267.59)	33.15	(426.49)
3 (push)	12.79	(164.57)	16.65	(214.18)	17.06	(219.52)	24.24	(311.83)	21.35	(274.68)	33.27	(428.05)
3 (pull)	9.53	(122.62)	16.28	(209.41)	13.59	(174.77)	22.26	(286.31)	18.81	(241.99)	25.35	(326.09)
4 (push)	12.77	(164.34)	16.64	(214.01)	18.36	(236.17)	26.55	(341.49)	22.53	(289.87)	33.39	(429.54)
4 (pull)	10.07	(129.56)	14.83	(190.84)	14.01	(180.22)	19.76	(254.17)	17.46	(224.59)	21.92	(281.94)

Table 11 Secant rotational stiffness for connection with HP pile /Type V and VI pad

Secant Rotational Stiffness [MN-m/rad (Kips-ft/degree)]								
Cycle No.	HP-BP1-V		HP-BP2-V		HP-BP1-VI		HP-BP2-VI	
1 (push)	9.49	(122.03)	10.74	(138.14)	33.81	(434.94)	63.27	(813.89)
1 (pull)	19.42	(249.81)	13.30	(171.15)	59.33	(763.25)	57.18	(735.64)
2 (push)	8.84	(113.79)	10.28	(132.29)	32.94	(423.78)	50.45	(648.98)
2 (pull)	13.17	(169.41)	11.73	(150.92)	32.87	(422.91)	45.85	(589.78)
3 (push)	7.66	(98.57)	11.88	(152.77)	25.89	(333.00)	36.30	(466.96)
3 (pull)	12.56	(161.62)	11.25	(144.71)	27.67	(355.96)	34.83	(448.09)
4 (push)	8.22	(105.76)	12.27	(157.79)	24.69	(317.57)	31.91	(410.49)
4 (pull)	13.56	(174.44)	11.43	(147.06)	25.51	(328.21)	30.74	(395.45)

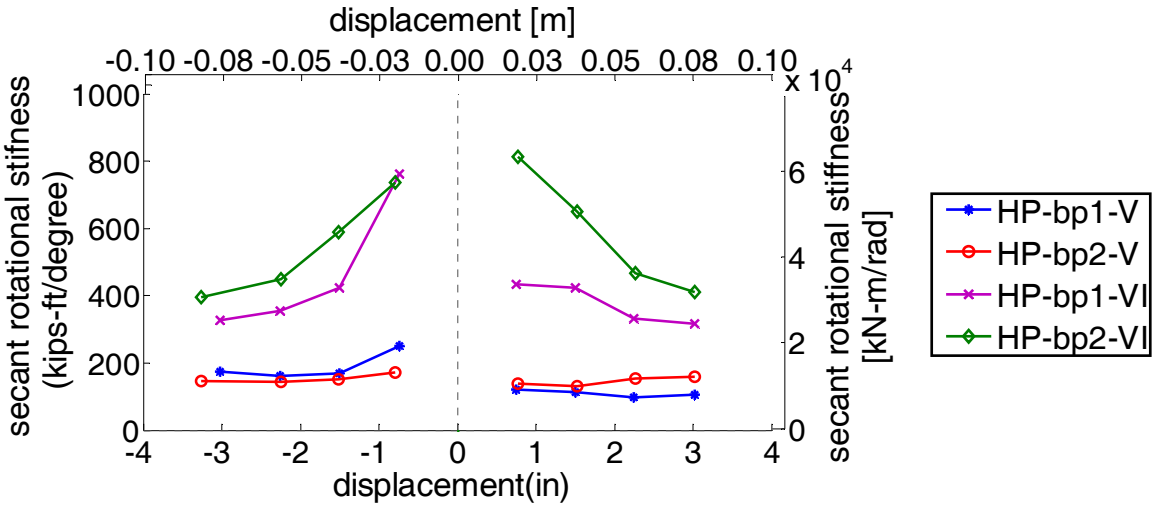

Fig. 18 Secant rotational stiffness of connection with HP pile for different axial load combinations (bp1, bp2 on Type V and VI pad)

The measured results were analyzed to determine the contribution of the various system components to the total top lateral displacement of the pile (Figure 19). Figures 20 to 21 show the contribution of the different elements to the overall displacement response of the system for selected cases. These figures show the contribution of each part to the top pile displacement for elastic cases of 76 mm (3 in). For the conditions tested, the girder rotation is the smaller contributor to the overall response and it increases for the circular pile cases. The

largest contributor to the overall response is the cap rotation. The bending of the pile is more significant when the pile is more flexible. The contribution by the shear deformation of the bearing pads to the response is around 2.5% to 7% for the majority of the cases.

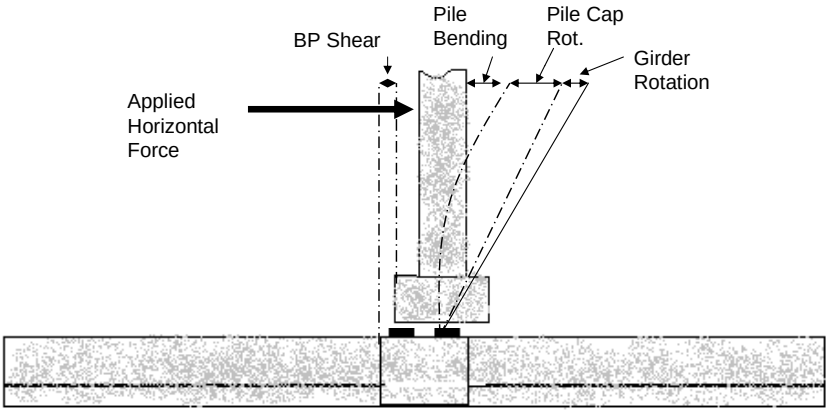

Figure 19. Components of contributing pile top displacement

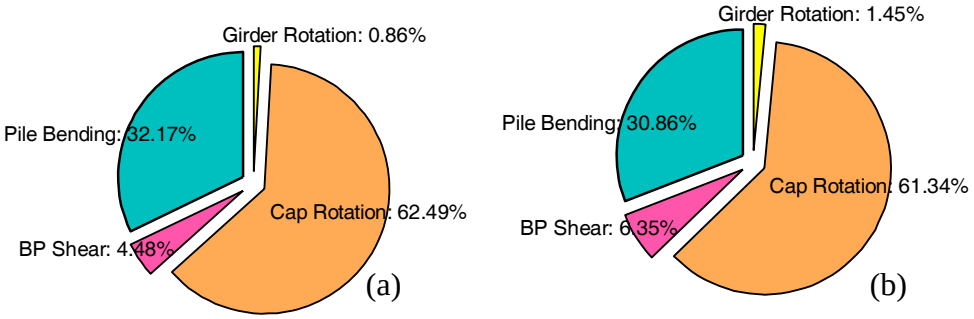

Fig. 20 Percent contribution of each element on top pile displacement for S4-BP3 (a) and S5-BP3 (b) cases

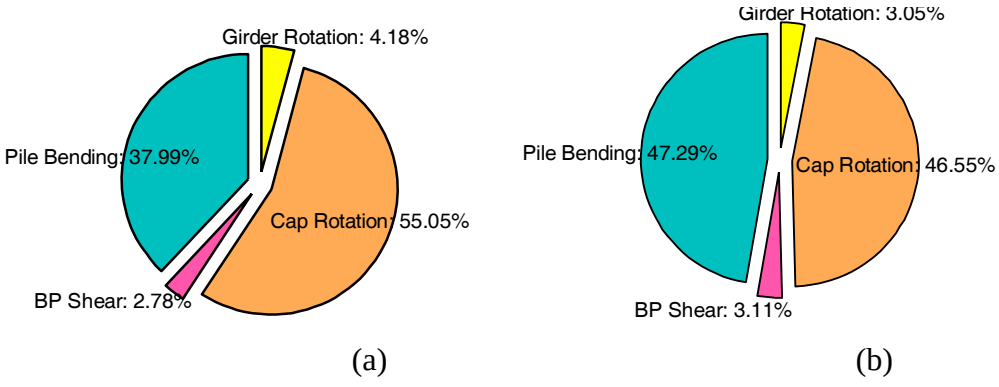

Fig. 21 Percent contribution of each element on top pile displacement for C4-BP3 (a) and C8-BP3 (b) cases

DESIGN RECOMMENDATIONS

The effective length factor (*K*) is "the factor that when multiplied by the equivalent length (L_e) yields the effective length for a stability (buckling) check of the pile" (Robinson et al, 2006). Equation (2) further defines the *K* factor.

$$K = L_b / L_e \tag{2}$$

L_e is effective length which can be defined as the distance from assumed fixed point of the pile (maximum moment) to the top of the pile. L_b is the effective length for a buckling check of the pile, defined as the total distance from one end of the pile to a first point of inflection along the deformed shape of the pile.

In an analysis of a pile top connection, there can be a variety of combinations of connections that will influence the *K*-factor. For a bridge bent, there is a point defined as the point of fixity in which the pile is assumed to be fixed in the ground based on where the maximum moment occurs due to lateral loads applied to the pile. Assuming that the pile is fixed in the ground at one end, three common pile connection assumptions are made with the super structure. It can be assumed to be free to move laterally and rotate (Figure 22 a), fixed to rotate but free to move laterally (Figure 22 b), or fixed from rotating and translating (Figure 22 c).

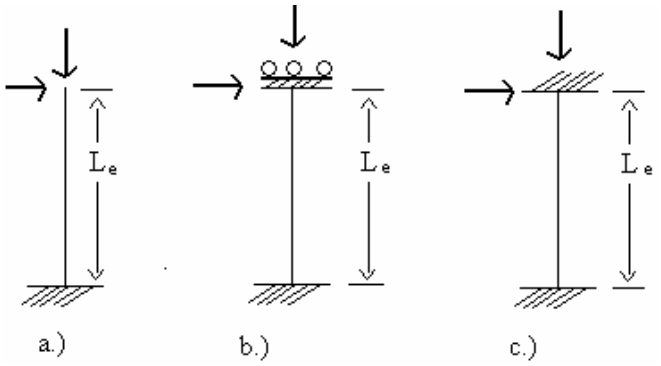

Fig. 22 (a-c) Pile connection model with applied horizontal and vertical loads (Gambhir, 2004)

When vertical and horizontal loads are applied to these connection types, the following deflected shapes are produced as shown in Figure 23 (a to c).

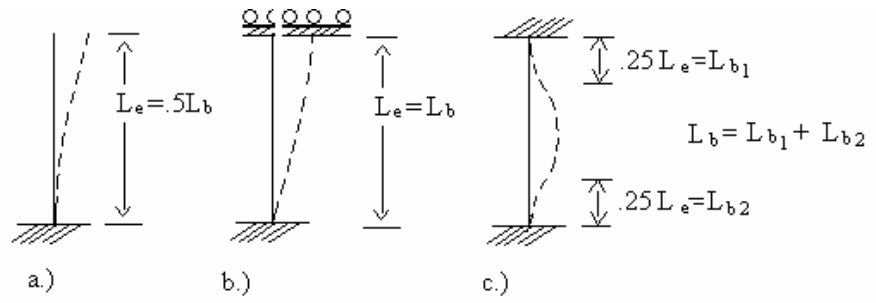

Fig. 23 (a-c) Deformed shape of piles due to lateral and vertical loading (Gambhir, 2004)

Knowing the appropriate lengths L_b and L_e, the *K*-factor can now be calculated for the three cases presented in Figures 20 and 21.

Case A:	**Case B:**	**Case C:**
$K = L_b / L_e = 2L_e / L_e = 2$	$K = L_b / L_e = L_e / L_e = 1$	$K = L_b / L_e = .5L_e / L_e = .5$

The effective length factor can be very useful for design application to determine the effective length for buckling of a pile segment. The bridge pile bents analyzed in this study are connected to the superstructure through anchor bolts and bearing pads. This connection type produces a *K*-factor that is somewhere from 0.5 to 2 presented for the three cases (A to C). In order to determine the appropriate K-factor for this type of connection, the points of inflection must be determined along the length of the pile for different pile configurations. From the data from full scale testing, the rotational, compressive, and shear stiffness of the pile due the bearing pad / anchor bolt connection can be inputted into pile analysis software such as FB-MultiPier (BSI, 2000) and modeled to calculate the moment along the length of the pile. By taking the slope at each point along the pile where the moment is calculated, the point of inflection can be determined by the maximum slope obtained. From these known points of inflection, the effective length for buckling for these cases can be measured and an appropriate *K*-factor can be determined for this type of connection. With an appropriate K-factor, the effective length for a proposed foundation element supporting a bridge with elastomeric bearing pad connections can be determined. In turn the calculated effective length of the foundation element can be used in a frame analysis to design the superstructure.

Example: <u>Step by Step K-factor calculation for a free head pile condition</u>

Figure 24 shows the step by step calculation of the effective length factor (K) with the proposed methodology for a pile with a free head condition. The values of equivalent or effective length (Le) and buckling length (L_b) were obtained from analyses of a nonlinear soil-pile model using FB-MultiPier. Additional information of the models can be found in Robinson et al (2006).

For cases in which the pile bents are connected to the superstructure through anchor bolts and bearing pads, rotational and translational springs have to be input into the soil-pile model and follow the same procedure discussed on Fig. 24 (a) and (b). The rotational spring constants can be obtained from Figures 14 to 17 or from Tables 6 to 11. For example, if the pile have an axial load of 241 kN (55 kips), bearing pad axial load is 86 kN (19.3 kips), applied lateral force of 71 kN (16 kips); then the rotational spring constant should be around 18.6 MN-m/rad (229.2 kips/degree). These values were obtained using the average rotational stiffness in both load directions (Case S3-BP1, Table 7).

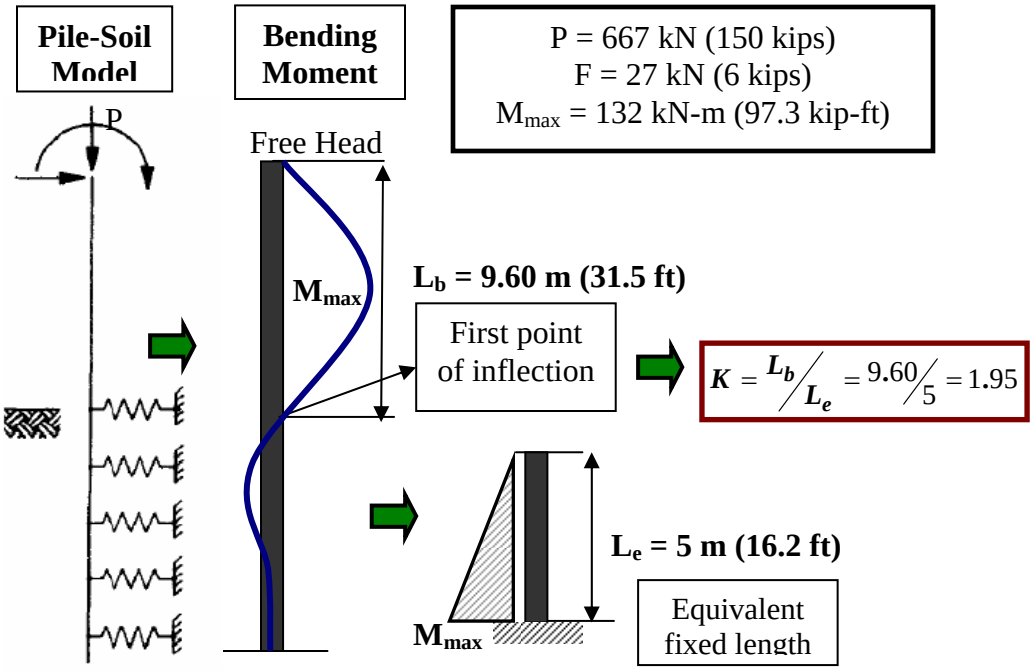

(a) Free Head

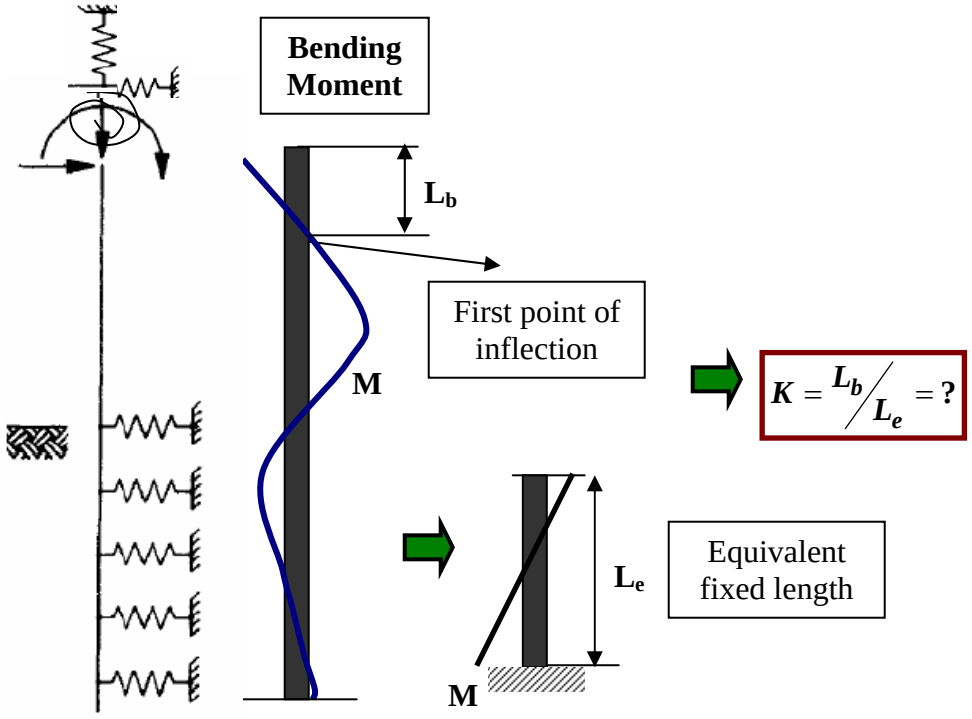

(b) Rotational and translational spring at top of pile

Fig. 24 Calculation of the K-factor

CONCLUSIONS

Several tests were performed on a typical connection of a bearing-supported bridge in the laboratory following details commonly used by NCDOT. The results show the capability of this type of connection to sustain the applied moments. It was able to develop the full strength of the pile. It was found from test observations that the weakest link of this connection was the steel sole plates located at the top of the bearing pads. As these plates bent, crushing of the concrete occurred at the diaphragm area. Under the applied lateral loads, the sole plates pull out the embedded plate on the girder. The embedded plate has four studs of 178 mm (7 in) in length, which provided enough strength against the pulling force produced by the bending of the sole plates experienced on these tests. The increase in the test pile and bearing pad stiffness caused by the increase in the axial loads also increased the rotational stiffness of the connection. For the conditions simulated in this testing program, the largest contributors to the overall displacement response of the tested system are the cap beam rotation, followed by the pile bending. Recommendations were proposed for evaluating effective length factors for bearing supported bridges that have a finite connection moment capacity.

FUTURE WORK

Using the design recommendations about effective length factors, a series of pile cases including a rotational spring at the top of the pile will be analyzed using FB-Multipier pile analysis software. In addition, the impact of these results on the substructure design will be determined. One of the desired outcomes will be the establishment of effective length or buckling factors for the pile foundation considering the type of boundary conditions imposed by the measured values of the rotational stiffnesses. Last, a model to predict the force-displacement response of this type of system will be developed.

ACKNOWLEDGEMENTS

This research was sponsored by the North Carolina Department of Transportation (NCDOT) Structures and Geotechnical divisions and North Carolina State University (NCSU). The valuable contributions of NCDOT engineers: Greg Perfetti, Tom Koch, Jeff Vones are acknowledged and greatly appreciated. Many thanks are expressed to all the staff and graduate students (Jerry Atkinson, Jonathan McEntire, William Dunleavy, Greg Lucier, Amy Yonai, Serena Hendrix, and Luis Montejo**)** of the Constructed Facilities Laboratory (CFL) at NCSU, where these tests were performed.

REFERENCES

Abendroth, R. E., Klaiber, F. W., and Shafer, M. W,''Diaphragm effectiveness in prestressed-concrete girder bridges,'' *Journal of Structural Engineering (ASCE)*, V. 121, No.9, September, 1995, pp.1362–1369.

Bridge Software Institute (BSI). (2000). FB-MultiPier Manual, Version 4. University of Florida, USA.

Eamon, C. and Nowak, A.,"Effect of secondary elements on bridge structural system reliability considering moment capacity", Structural Safety ,V. 26, February, 2004, pp. 29–47

Gambhir,M.L. "Stability Analysis and Design of Structures." Springer, 2004.

Green, T., Yazdani, N., and Spainhour, L.,"Contribution of intermediate diaphragms in enhancing precast bridge girder performance", *Journal of performance of constructed facilities (ASCE),*V. 18, No. 3, August, 2004, pp. 142-146.

Robinson, B., Suarez, V., Robalino, P., Kowalsky, M. and Gabr, M., "Pile Bent Design Criteria." *NCDOT Research Project 2005-19*. Report no. FHWA/NC/2006-14. June, 2006.

Yazdani, N., Scott, E., and Chun, C.,"Effect of bearing pads on precast prestressed concrete bridges", *Journal of Bridge Engineering (ASCE),* V. 5, No.3,August, 2000, pp. 224-232.

Yoon, D.Y., Yoo, C.H., and Lee, S.C., "On the behavior of sole plates in steel girders", *Thin-Walled Structures*, V. 42, No.1, January, 2004, pp. 59-77.

www.ncdot.org